Optimal control applications in blood flow simulations

TELMA GUERRA[1] JORGE TIAGO[2] ADÉLIA SEQUEIRA[3]

Abstract. Blood flow simulations can be improved by integrating known data into the numerical simulations. Data assimilation techniques based in a variational approach can have an important role on this. We propose a nonlinear optimal control problem to reconstruct a blood flow profile in 2D stenosis geometries from partial observations of known data. The cost function includes a misfit for the wall shear stress, considered an important indicator for medical purposes. We assume the blood to have a non-Newtonian behavior. Using a discretize then optimize approach, we solve the nonlinear optimal control problem and we propose a weighted cost function that accurately recovers both the velocity and wall shear stress profiles. We test the robustness of such cost function with respect to different velocity profiles and degrees of stenosis. The filtering effect of the method is also confirmed. We conclude that this approach can be successfully used for the 2D case.

Keywords. Optimal control; Non-Newtonian fluids; Data Assimilation.

AMS Subject Classification.

1 Introduction

Nowadays medical community and scientists join efforts and work together with the purpose of providing numerical simulations of the cardiovascular system for healthy and sick human being. The collaboration between the medical community and scientists offers not only an exchange of knowledge between both

[1]Escola Superior de Tecnologia do Barreiro, IPS. E-mail:telma.guerra@estbarreiro.ips.pt.
Centro de Matemática e Aplicações, FCT-UNL.
[2]IST. E-mail:jorge.tiago@math.ist.utl.pt.
Cemat.
[3]IST. E-mail:adelia.sequeira@math.ist.utl.pt.
Cemat.

strands but also an exchange of data information that can be used by the scientists in the numerical simulations to predict the blood behavior under healthy or disease conditions.

The progress of medical imaging techniques, blood flow modelling, and computational capacity allow us to consider the possibility of obtaining patient specific simulations. If such tools are available to medical community, then the advantages in therapy prediction, training and expenses reduction can be very significant. In order to obtain such accuracy, data information must be included in the numerical simulations. This procedure is known in the literature as Data Assimilation (DA). Other engineering fields like geophysics and meteorology know very well these techniques. However recent work ([7, 8]) has shown that they can also be successfully used while simulating blood flow.

One of the most frequent disease, in the cardiovascular system, is atherosclerosis, which gives rises to a stenosis by partially obstructing the artery. This reduction in the vessels diameter commits the normal behavior of the blood circulation. Also, although not fully understood yet, it is already known that hemodynamical aspects, like the shear stress exerted by the blood flow on the vessels walls, can affect the progression of this and other pathologies (see [6, 18, 3]).

In normal situations the blood flow has a Newtonian behavior in most parts of the arterial system. In fact, when non-Newtonian effects are observed it may indicate that some abnormality can be occurring. Some examples of such effects are the observation of a more stable recirculation of the flow downstream a stenosis or inside a saccular aneurysm. In such cases it is important the study of non-Newtonian behavior as well as shear-thinning viscosity, thixotropy and eventually the yield stress of the blood. This behavior is related to the properties of red blood cells, namely its tendency to form tri-dimensional structures at low shear rates and to align in blood flow direction at high shear rates ([23, 22]).

In this paper we would like to focus on the above aspects of blood flow. In this sense, we propose and validate a DA method, based on a variational approach ([7]), to numerically reconstruct the blood flow in 2D idealized stenosis, while assuming a non-Newtonian rheology. In the DA method we take into account the Wall Shear Stress (WSS) and we verify that this leads to better precision in a posterior measurements. We validate the robustness of the method with respect to the stenosis degree and to different flow profiles. Additionally we verify the filtering effect of the DA process.

The paper is organized as follows. In section 2 we describe the mathematical model that will be used later in the numerical simulations. In the section 3 we describe the DA procedure as a variational frame, which is our choice for DA implementation and we state the derived control problem formulation. Section 4 is essentially devoted to the discretization of the optimal control problem following the discretize then optimize approach. The numerical results for the choice and robustness of the cost function parameters are reported in section 5. Finally, we summarize our conclusions in section 6.

2 Dynamic equations and viscosity models

Along this work, the blood flow is modeled as an incompressible and laminar flow whose dynamic equations derive from classical mechanics principles: mass conservation and conservation of linear momentum. These equations describe the fluids motion in an domain of interest $\Omega \subset I\!R^2$ and can be written as

$$\begin{cases} \rho\left(\dfrac{\partial \mathbf{y}}{\partial t} + (\mathbf{y}\cdot\nabla)\mathbf{y}\right) - div\,(\tau(D\mathbf{y})) + \nabla p = \mathbf{f} & \text{in } \Omega \\ div\,\mathbf{y} = 0 & \text{in } \Omega \end{cases} \tag{1}$$

with suitable boundary conditions. The control and state variables are constrained to satisfy a system with shear dependent viscosity which decreases when the shear rate grows (shear-thinning). The unknowns are the velocity field $\mathbf{y}$ and the pressure p. The density of the fluid is represented by ρ and $\mathbf{f}$ is the given body force. The viscous stress tensor is represented by

$$\tau = 2\mu(\dot{\gamma})D\mathbf{y}$$

where μ is the kinematic viscosity, $\dot{\gamma}$ is the shear rate given by

$$\dot{\gamma} = \sqrt{\frac{1}{2}(\nabla\mathbf{y} + (\nabla\mathbf{y})^T) : (\nabla\mathbf{y} + (\nabla\mathbf{y})^T)} = \sqrt{2}|D\mathbf{y}|\,,$$

and D is the strain tensor

$$D\mathbf{y} = \frac{1}{2}\big(\nabla\mathbf{y} + (\nabla\mathbf{y})^T\big)\,,$$

that is, the symmetric part of the velocity gradient.

For Newtonian flow, τ is a linear function depending on $D\mathbf{y}$ once μ is a constant. This property does not happen for non-Newtonian flow. In such cases, μ is a non-linear function of the stress tensor, leading to difficulties in the treatment of the non-linearities in addition to the convective term that has also a non-linear nature.

Our blood flow simulations compare both $2D$ Newtonian and non-Newtonian models for the stationary case where we get $\dfrac{\partial \mathbf{y}}{\partial t} = 0$ in equation (1). For non-Newtonian models we capture the shear-thinning viscosity effects in the flow which corresponds to a decreasing viscosity as the shear rate grows.

Viscosity functions can be written in the general form

$$\mu(\dot{\gamma}) = \mu_\infty + (\mu_0 - \mu_\infty)F(\dot{\gamma}) \tag{2}$$

where μ_0 and μ_∞ are the asymptotic viscosity values at zero and at infinite shear rates and $F(\dot{\gamma})$ is a bounded function depending on the shear rate. The function F goes to one at zero shear rate and goes to zero at infinite shear rate. Different choices for F correspond to different models for blood flow.

The choice of the correct viscosity blood is important to obtain accuracy in blood flow simulations and the viscosity parameters related to each model have to be choosen accordingly our specific model and taking account the temperature, hematocrit and healthy of the individual donor ([23, 25]).

In [10], the authors used known estimates to converte data and obtain realistic viscosity values at 37°C. Comparing data with viscosity models, they obtained the constants for each model using non-linear least squares fitting of the viscosity data. Despite the absence of data for μ_0, the authors concluded that Carreau and Cross models fit very well the experimental data.

Based on their conclusions, for the $2D$ stenosis case, we considered

$$F(\dot{\gamma}) = \frac{1}{(1 + (\lambda\,\dot{\gamma})^b)^a}\,,$$

for $a, b, \lambda > 0$ hence (2) becomes

$$\mu(\dot{\gamma}) = \mu_\infty + \frac{\mu_0 - \mu_\infty}{(1 + (\lambda\,\dot{\gamma})^b)^a}\,, \tag{3}$$

which is usually known as generalized Cross model.

3 The DA method

In this section we are going to describe our approach to the DA problem. Our goal is to obtain numerical solutions for problem (1) which coincides, within a certain error, to observed data measured at certain parts of the domain. Different techniques may be used for this purpose, namely the so called variational approach, matrix updating or domain splitting, both at the discrete level. In [9] the variational approach is shown to be superior to the remaining methodologies. The variational approach is based on the assumption that we are free to adjust or control some of the model parameters and chose among the corresponding solution, according to some criteria. In the simplest frame such criteria corresponds to misfit

$$\int_{\Gamma_{part}} |\mathbf{y} - \mathbf{y}_d|^2 \, dx$$

between the obtained solution $\mathbf{y}$ and the data $\mathbf{y}_d$ measured over a subdomain Γ_{part}. By taking the adjustable parameters as a control function $\mathbf{u}$ defined on Ω_c, possibly different from Γ_{part}, we are then facing an optimal control problem which also corresponds to an inverse problem. It is known that, when dealing with linear models, the possible ill-posedness (non uniqueness) of such inverse problem can be avoid by adding to the criteria a regularizing term like

$$\int_{\Omega_c} |\mathbf{u}|^2 \, dx \quad \text{or} \quad \int_{\Omega_c} |\nabla \mathbf{u}|^2 \, dx \, .$$

Using such type of cost functions will allow to prove, within certain assumptions, the uniqueness of solution for the corresponding optimal control problem.
Here we assume that our domain Ω represents an artery truncated by two artificial boundaries Γ_{in} and Γ_{out}, the inlet and outlet respectively, as represented in figure 1.

Our control function corresponds to the inlet velocity profile. We also assume that the data corresponds to the velocity observed at part $\Gamma_{part} \subset \Omega$. Additionally, we can assume to know the WSS at part of the boundary Γ_{wall}. In fact,

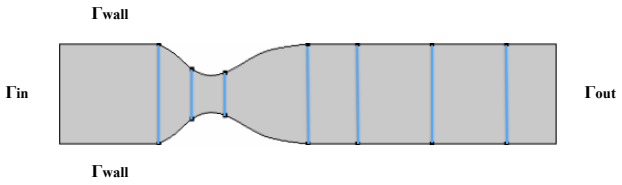

Figure 1: Domain representation

as mentioned in section 1, the WSS is an important indicator for monitoring certain pathologies. Therefore it is desirable that the DA method can accurately reconstruct the desired WSS. In this sense we also include the misfit

$$\int_{\Gamma_{wall}} |w - w_d|^2$$

between the obtained WSS magnitude w and w_d the registered WSS magnitude. Note that the WSS is the tangential component of the stress exerted by the fluid in the vessels wall so that it can be given by

$$WSS = \sigma_n - (\sigma_n \cdot \mathbf{n})\mathbf{n}\,, \tag{4}$$

where $\mathbf{n}$ is the outward normal to the wall surface and $\sigma_n = \sigma\mathbf{n}$ is often called the normal component of the stress tensor σ. Assuming $\sigma = p\mathbf{I} - \tau$, (4) can be written as

$$WSS = \mu(\nabla\mathbf{y} + (\nabla\mathbf{y})^T)\mathbf{n} - \mu[((\nabla\mathbf{y} + (\nabla\mathbf{y})^T)\mathbf{n}) \cdot \mathbf{n}]\mathbf{n}\,. \tag{5}$$

We resume the DA method as solving the optimal control problem

$$\min_u \mathbf{J}(\mathbf{y}, \mathbf{u}) = w_1 \int_{\Gamma_{part}} |\mathbf{y} - \mathbf{y}_d|^2\, dx + w_2 \int_{\Gamma_{wall}} |w - w_d|^2\, dx + w_3 \int_{\Gamma_{in}} |\nabla\mathbf{u}|^2\, dx \tag{6}$$

subject to

$$\begin{cases} -div\,\tau + \rho(\mathbf{y}\cdot\nabla)\mathbf{y} + \nabla p = \mathbf{f} & \text{in } \Omega \\ div\,\mathbf{y} = 0 & \text{in } \Omega, \\ \mathbf{y} = 0 & \text{on } \Gamma_{wall} \\ \mathbf{y} = \mathbf{u} & \text{on } \Gamma_{in} \\ -\sigma\mathbf{n} = 0 & \text{on } \Gamma_{out}. \end{cases} \tag{7}$$

The weights w_1, w_2 and w_3 should be chosen such that problem (6 - 7) admits a solution (preferable unique).

Up to the authors knowledge, problem (6 - 7) was not studied concerning the existence of solution, even for the quadratic cost functional obtained by taking $w_2 = 0$. In fact, optimal control problems for non-Newtonian fluids have been studied only for recent years. For the two-dimensional steady case we mention [4] for boundary control of quasilinear elliptic equations, and [5, 24] both for distributed control. For two-dimensional unsteady case, we refer [26], and for three-dimensional coupled modified Navier-Stokes and Maxwell equations, [13]. Further, for distributed control on three-dimensional domains we cite [1] and [11]. None of the cited authors focused on the boundary control problem for the nonlinear system (7).

In spite of lacking an appropriate theoretical frame, we assume enough regularity on the problem variables and we propose a numerical approach to solve the problem. This will be the subject of the next section.

4 Discretization and SQP method

To solve an optimal control problem numerically, we can adopt either the Discretize then Optimize (DO) approach or the Optimize then Discretize (OD). There is still some controversy on which, if any, is better then the other. Here we follow the work of [7] whose authors preferred the DO to the OD (see, for instance, [12] for some comments on this).

The DO consists in first discretizing the optimal control problem and then solve the finite dimensional optimization problem resulting from the discretization. For the first step we use typical FEM that reads as follows. We first address the weak formulation of (1) for the steady case.

Let us assume that we are looking for $\mathbf{y} \in \mathbf{H}^1(\Omega)$ and for $p \in \mathbf{L}^2(\Omega)$. We consider $\mathbf{V} = \{\mathbf{v} \in \mathbf{H}^1(\Omega) : \ \mathbf{v}|_{\partial\Omega_D} = 0\}$, with $\partial\Omega_D = \Gamma_{in} \cap \Gamma_{wall}$, and $\mathbf{Q} = \mathbf{L}^2(\Omega)$ as the spaces of test functions corresponding to $\mathbf{y}$ and p respectively. Multiplying (1) by suitable test functions and integrating by parts we obtain

$$\begin{cases} \int\limits_\Omega \tau(D\mathbf{y}) : \nabla\mathbf{v} + \int\limits_\Omega (\rho(\mathbf{y}\cdot\nabla)\mathbf{y})\cdot\mathbf{v} - \int\limits_\Omega p\, div\, \mathbf{v} = \int\limits_\Omega \mathbf{f}\cdot\mathbf{v} \\ \\ \int\limits_\Omega q\, div\, \mathbf{y} = 0 \end{cases} \tag{8}$$

for all $\mathbf{v} \in \mathbf{V}$ and $q \in \mathbf{Q}$.
Let us consider the finite dimensional subspaces $\mathbf{V}_h \subset \mathbf{V}$ and $\mathbf{Q}_h \subset \mathbf{Q}$ with $h > 0$, $dim(\mathbf{V}_h) = N_y$ and $dim(\mathbf{Q}_h) = N_p$. We then take the finite dimensional approximations

$$\mathbf{y}_h = \sum_{j=1}^{N_y} y_j\phi_j \in \mathbf{V}_h, \quad p_h = \sum_{k=1}^{N_p} p_k\psi_k \in \mathbf{Q}_h \tag{9}$$

where ϕ_j and ψ_k are the shape functions belonging to $\mathbf{V}_h$ and $\mathbf{Q}_h$ respectively. The coefficients y_j and p_k are unknown constants to be determined.
Considering that the space of the shape functions coincides with the space of the test functions, we reach the following approximated problem: find $\mathbf{y}_h \in \mathbf{V}_h$ and $p_h \in \mathbf{Q}_h$ such that

$$\begin{cases} \int\limits_\Omega \tau(D\mathbf{y}_h) : \nabla\mathbf{v}_h \quad + \int\limits_\Omega (\rho(\mathbf{y}_h\cdot\nabla)\mathbf{y}_h)\cdot\mathbf{v}_h - \int\limits_\Omega p_h\, div\, \mathbf{v}_h \\ \qquad\qquad\qquad\qquad = \int\limits_\Omega \mathbf{f}\cdot\mathbf{v}_h \\ \\ \int\limits_\Omega q_h\, div\, \mathbf{y}_h = 0\,. \end{cases} \tag{10}$$

If we chose $\mathbf{V}_h$ and $\mathbf{Q}_h$ correctly then it is possible to prove the existence of solution for the approximated problem and to check that $(\mathbf{y}_h, p_h)$ converges to the solution $(\mathbf{y}, p)$ of (8).
The Finite Element Method theory (FEM), when applied to flow modelling, gives us such spaces. Here we use the well known spaces corresponding to the

Taylor-Hood elements ($P2$-$P1$), both for shape and test functions. We can now proceed to the space discretization.
First, let us consider the convective term

$$\int_\Omega (\rho(\mathbf{y}_h \cdot \nabla)\mathbf{y}_h) \cdot \mathbf{v}_h \, .$$

Substituting $\mathbf{y}_h$ by the corresponding finite approximation (9) and $\mathbf{v}_h$ by the test functions $\phi_i,\ i = 1...N_y$ we obtain

$$\int_\Omega \left[\left(\rho \sum_{j=1}^{N_y} y_j \phi_j \cdot \nabla \right) \sum_{k=1}^{N_y} y_k \phi_k \cdot \phi_i \right], \ i = 1...N_y \, .$$

After some computations we have that the convective term can be written as

$$\left(\sum_{j=1}^{N_y} y_j \sum_{k=1}^{N_y} y_k \int_\Omega (\rho \phi_j \cdot \nabla)\phi_k \cdot \phi_i \right)_{i=1...N_y} = \mathbf{G}(Y)Y$$

where $Y = (y_1, ..., y_{N_y})^T$ and

$$\mathbf{G}(\mathbf{Y}) = \sum_{k=1}^{N_y} y_k \int_\Omega (\rho \phi_j \cdot \nabla)\phi_k \cdot \phi_i \, .$$

We now turn our attention to the viscous stress tensor τ. The term we want to discretize is

$$\int_\Omega \tau(D\mathbf{y}_h) : \nabla \mathbf{v}_h$$

where the tensor can be written as

$$\tau = 2\mu(|D\mathbf{y}|)D\mathbf{y},$$

and μ is the Cross model for viscosity given by (3).
Replacing $\mathbf{y}_h$ by its corresponding finite approximation we have

$$\left(\int_\Omega 2\mu\Big(\Big|\sum_{j=1}^{N_y} \mathbf{y}_j D\phi_j\Big|\Big) \sum_{k=1}^{N_y} \mathbf{y}_k D\phi_k : \nabla\phi_i \right)_{i=1\dots N_y} = \mathbf{Q}(Y)\,.$$

Hence system (10) becomes

$$\begin{cases} \mathbf{Q}(Y) + \mathbf{G}(Y)Y + B^T P = F \\ BY = 0\,. \end{cases} \tag{11}$$

As for the cost function (6), we discretize it using again the FEM basis functions. Assuming that a mesh of Ω is fixed, we refer to the basis functions associated to the nodes in Γ_{part} as $(\phi_i)_{i=1\dots N_o}$ and to those on Γ_{in} as $(\phi_i)_{i=1\dots N_u}$. The approximated control function is then defined by

$$\mathbf{u}_h = \sum_{j=1}^{N_u} u_j \phi_j\,.$$

To discretize the first term we replace both $\mathbf{y}$ and $\mathbf{y}_d$ by their respective finite dimensional approximations $\mathbf{y}_h$ and $\mathbf{y}_{d_h}$ given by

$$y_{h_d} = \sum_{i=1}^{N_0} y_{d_i}\phi_i\,.$$

We then obtain

$$\begin{aligned}
&\int_{\Gamma_{part}} \left\langle \sum_i^{N_o} (\mathbf{y}_i - \mathbf{y}_{d_i})\phi_i,\ \sum_j^{N_o} (\mathbf{y}_j - \mathbf{y}_{d_j})\phi_j \right\rangle dx \\
&= \int_{\Gamma_{part}} \sum_i^{N_o} (\mathbf{y}_i - \mathbf{y}_{d_i}) \sum_j^{N_o} (\mathbf{y}_j - \mathbf{y}_{d_i}) \left\langle \phi_i, \phi_j \right\rangle dx \\
&= \sum_i^{N_o} (\mathbf{y}_i - \mathbf{y}_{d_i}) \sum_j^{N_o} (\mathbf{y}_j - \mathbf{y}_{d_i}) \int_{\Gamma_{part}} \phi_i\phi_j\, dx \\
&= (Y - Y_d)^T \mathbf{M}^1 (Y - Y_d) = \left\langle (Y - Y_d)^T, \mathbf{M}(Y - Y_d) \right\rangle \\
&= \|Y - Y_d\|_{N_y}
\end{aligned} \tag{12}$$

where $\|\cdot\|_{N_y}$ is the norm induced by the inner product $<\cdot, \mathbf{M}\cdot>$ and $\mathbf{M}$ is a symetric $N_y \times N_y$ matrix such that each element is given by

$$m_{ij} = \int_{\Gamma_{part}} \phi_i \phi_j \, dx \, .$$

We now turn our attention to the term related to the WSS. Taking (5) into account we have

$$w = \sqrt{2\mu(|D\mathbf{y}|)D\mathbf{y}\,\mathbf{n} - [2\mu(|D\mathbf{y}|)(D\mathbf{y}\,\mathbf{n})\cdot\mathbf{n}]\mathbf{n}} \, .$$

Since w will be evaluated on the no-slip boundary, $D\mathbf{y}$ must be approximated by an expression $D(Y)$ depending on neighbourhood elements where the velocity doesn't vanish. Such expression can be obtained using finite differences or an inheritance based averaging method ([19]). Then the approximation for w_h can be writen as

$$w_h(Y) = \sqrt{2\mu\left(D(Y)\right)\left(D(Y)\,\mathbf{n} - (D(Y)\,\mathbf{n}\cdot\mathbf{n})\,\mathbf{n}\right)} \, .$$

Proceeding similarly for the observed WSS w_d we can approximate

$$\int_{\Gamma_{wall}} |w - w_d|^2 \, dx$$

by

$$\int_{\Gamma_{wall}} \left| w_h - w_{h_d} \right|^2 = \mathbf{W}(Y) \tag{13}$$

where $\mathbf{W}$, obtained by a gaussian quadrature rule, depends nonlinearly on Y. Finally, for the regularization term we have

$$\begin{aligned} \int_{\Gamma_{in}} |\nabla \mathbf{u}|^2 \, dx &= \int_{\Gamma_{in}} \left| \sum_i \mathbf{u}_i \nabla \phi_i \right|^2 dx = \int_{\Gamma_{in}} \left\langle \sum_i \mathbf{u}_i \nabla \phi_i, \sum_j \mathbf{u}_j \nabla \phi_j \right\rangle dx \\ &= \sum_i \mathbf{u}_i \sum_j \mathbf{u}_j \int_{\Gamma_{in}} \nabla \phi_i \nabla \phi_j = U^T \mathbf{A} U = \left\langle U^T, \mathbf{A}U \right\rangle = \|U\|_{N_u} \end{aligned} \tag{14}$$

where $\|\cdot\|_{N_u}$ is the norm induced by the inner product $<\cdot, \mathbf{A}\cdot>$ and $\mathbf{A}$ is a symetric $N_u \times N_u$ matrix such that each element is given by

$$a_{ij} = \int_{\Gamma_{in}} \nabla\phi_i \nabla\phi_j \, dx \, .$$

Taking account (4), (12), (13) and (14), the discrete version of the control problem (6 - 7) becomes

$$J(Y,U) = \|Y - Y_d\|_{N_y} + \mathbf{W}(Y) + \|U\|_{N_u} \tag{15}$$

subject to

$$\begin{cases} \mathbf{Q}(Y) + \mathbf{G}(Y)Y + B^T P = F \\ BY = 0 \, . \end{cases} \tag{16}$$

4.1 Sequential Quadratic Programming

The mathematical programming problem (15 - 16) is nonlinear problem both with respect to the cost function and constraints. To solve this problem we use a particular Sequential Quadratic Programming (SQP) approach implemented in the package Sparse Nonlinear Optimization (SNOPT) which we describe here briefly (see ([15, 20])).

First a major step is required to approximate the nonlinear problem by a quadratic programming problem (QP). The constraints of such approximation correspond to the linearization of (16). The quadratic cost is a second order approximation to the modified Lagrangian function associated to (15 - 16). The Hessian matrix is replaced by a quasi-Newton approximation obtained by a BFGS uptade. The second step consists in solving the (QP) problem which is done by a reduced-Hessian iterative method implemented in SQOPT ([17]). The solution of the approximation (QP) is used to compute a descent direction for (15 - 16). A line search method is then executed to find the new solution for the nonlinear problem.

The strength of this approach is the fact that it has been tested in large scale nonlinear optimization problems with up to 40000 variables ([15]).

5 Numerical results

As known data y_d and w_d we used synthetic data generated numerically. For this purpose, we considered a 2D stenosed vessel (see figure 1) with length iqual to $L = 2R$, maximum diameter $D = 2R$ and minimum diameter $d = R$ using $R = 3.1mm$, which is closed to fisiological measures ([2]). For the fluid model we considered the generalized Cross model, as described in section 2, with boundary conditions defined as in (7). The parameters for the generalized Cross model were chosen as in [2]:

$$\mu_0 = 1.6e^{-1}\, Pa.s, \quad \mu_\infty = 3.6e^{-3}\, Pa.s$$

$$a = 1.23, \quad b = 0.64, \quad \lambda = 8.2\, s$$

$$\rho = 1059\, Kg/m^3\,.$$

To construct and to treat our working domains we resort to COMSOL Multiphysics. Using the available options for Laminar Flow, we built a mesh composed by 3398 triangular and quadrilateral elements with 15986 degrees of freedom (dofs) for the velocity. The quadrilateral elements were used to refine the mesh along the no-slip boundaries, the regions of boundary layers. The minimum element quality registered was 0.2628 and the average element quality was 0.8262 (maximum is 1).

The fluid model was solved by imposing a Poiseuille velocity profile at the inlet with a mean velocity given by $U_0 = 0.0993\, m/s$, which corresponds to a Reynold's number of 180. The non-linear problem was treated with Newton´s method while each resulting linear system was solved using the direct solver PARDISO. Also we set that the nested dissection method should be used, as a preordering algorithm, to minimize the zero elements after the factorization. Such methods are also available with COMSOL Multiphysics.

In figure 2 we represent the velocity magnitude obtained as described before where we highlight the recirculation region that apear dowstream the stenosis. We compare it with the Newtonian case where we took the viscosity equal to μ_∞. These results are consistent with [2] despite the stenosis are not exactly equal.

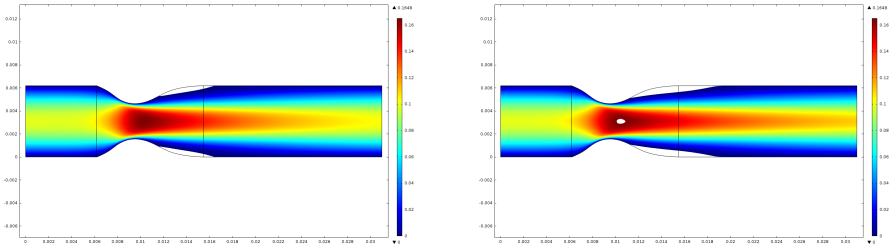

Figure 2: Data velocity highlighting the recirculation region. Leff: non-Newtonian case, right: Newtonian case.

The figure 3 represents the magnitude of the WSS for the non-Newtonian case. We can observe a high increase of the magnitude value in the area of partial obstruction of the flow, when comparing with the remain vessel.

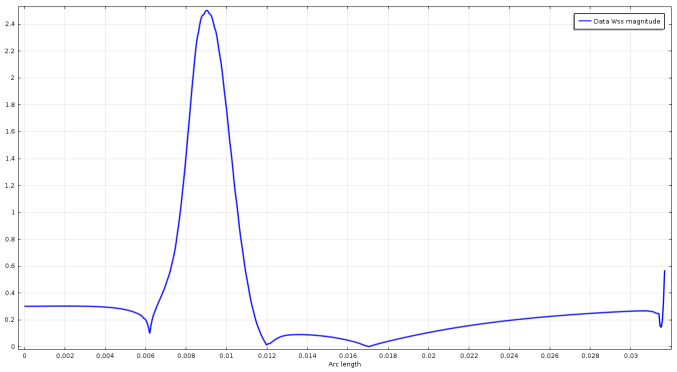

Figure 3: Data WSS magnitude

5.1 Parameters Testing/choice

The cost function (6) plays an important role in the performance of the DA method. It depends both on the observed domain Γ_{part} and on the weighting parameters w_1, w_2 and w_3. Choosing correctly the observed domain is an important issue (see [14]) and it was treated for the discrete linearized Navier-Stokes equations in [7], where Γ_{part} was considered to be a finite number of points. Here we don't deal with this issue, and we assume that $\mathbf{y}_d = \mathbf{y}_d(x, y)$ is fully determinate over Γ_{part}, which corresponds to the vertical blue lines represented in figure 1. We will be concerned, however, with the choice of the weighting parameters for the cost function.

It is classical that proper balance of the terms in a quadratic type cost function

($w_2 = 0$) can be treated by Tikhonov's regularization techniques (see [7] for some applications). But, up to the authors knowledge, such techniques can not be easily applied for a nonlinear cost function like (15). Therefore we present an heuristic numerical study to investigate which set of parameters (w_1, w_2, w_3) provides a better approximation of the data, including the velocity, the WSS and, through the optimal control variable, the inlet profile.

In order to solve each problem of the type (15 - 16) we use the SQP method implemented in SNOPT, as briefly described in section 4.1. To compute the gradient of the cost function with respect to the control variables we used the adjoint method ([19]). The optimality tolerance, which determines the accuracy for the approximation of first-order optimality conditions ([16]), was fixed in $1e^{-6}$. For the QP solver, we imposed that the Cholesky factor of the reduced Hessian should be kept. The control problems were solved using the mesh described above and taking 37 degrees of freedom for the control variable imposed on the inlet boundary.

Table 1: Cost function terms values fixing w_2 and w_3 and varying w_1.

	$\int_{\Gamma_{part}} \lvert Y\rvert^2$	$\int_{\Gamma_{wall}} \lvert W\rvert^2$	$\int_{\Gamma_{in}} \lvert\nabla \mathbf{u}\rvert^2$	CF
$(0, 1e^6, 1e^{-3})$	$4.152000e^{-7}$	$1.838053e^{-13}$	8.190109	0.0081902934
$(1e^5, 1e^6, 1e^{-3})$	$2.049161e^{-11}$	$2.284326e^{-16}$	8.477968	0.0084800177
$(1e^6, 1e^6, 1e^{-3})$	$2.196835e^{-13}$	$6.982916e^{-18}$	8.481701	0.0084819206
$(1e^7, 1e^6, 1e^{-3})$	$2.225967e^{-15}$	$1.029709e^{-19}$	8.482097	0.0084821196

We can see the quantitative results in the tables 1, 2 and 3 where we take $Y = \mathbf{y} - \mathbf{y}_d$, $W = w - w_d$ and CF to represent the final cost function value. We

Table 2: Cost function terms values fixing w_1 and w_3 and varying w_2.

	$\int_{\Gamma_{part}} \lvert Y\rvert^2$	$\int_{\Gamma_{wall}} \lvert W\rvert^2$	$\int_{\Gamma_{in}} \lvert\nabla \mathbf{u}\rvert^2$	CF
$(1e^6, 0, 1e^{-3})$	$2.229353e^{-13}$	$4.493504e^{-13}$	8.481696	0.0084819189
$(1e^6, 1e^5, 1e^{-3})$	$2.198003e^{-13}$	$6.444382e^{-16}$	8.481701	0.0084819206
$(1e^6, 1e^7, 1e^{-3})$	$2.196719e^{-13}$	$7.027137e^{-20}$	8.481701	0.0084819206

Table 3: Cost function terms values fixing w_1 and w_2 and varying w_3.

	$\int_{\Gamma_{part}} \lvert Y\rvert^2$	$\int_{\Gamma_{wall}} \lvert W\rvert^2$	$\int_{\Gamma_{in}} \lvert\nabla \mathbf{u}\rvert^2$	CF
$(1e^6, 1e^6, 1e^{-5})$	$7.794634e^{-14}$	$1.479646e^{-16}$	8.529495	$8.53730414e^{-5}$
$(1e^6, 1e^6, 1e^{-4})$	$2.224927e^{-15}$	$1.898105e^{-21}$	8.482097	$8.48211969e^{-4}$
$(1e^6, 1e^6, 1e^{-2})$	$2.052022e^{-11}$	$2.194004e^{-14}$	8.477961	0.0848001567
$(1e^6, 1e^6, 1e^{-1})$	$1.727427e^{-9}$	$2.725338e^{-11}$	8.445729	0.8463276594
$(1e^6, 1e^6, 0)$	$6.029549e^{-14}$	$9.237606e^{-17}$	171.890855	$6.03878696e^{-8}$
$(1e^6, 1e^6, 1e^1)$	$4.600914e^{-6}$	$3.811922e^{-6}$	6.645082	74.863651813

can check that both the velocity and the WSS are better approximated when all the parameters are non null.

Also, in table 1 we can notice that, as expected, better results for velocity and WSS are attained when w_1 is increased. Such increase requires a growing number of SNOPT iterations to solve (15 - 16). Therefore, we only present results obtained for less then 400 iterations. If we consider $w_1 = 0$, the resulting cost function has the worst performance in approximating the velocity and one of the worst for WSS. Maintaining w_1 and w_3 and increasing w_2, in table 2 we can observe that better results for WSS are attained and for velocity also even

though less expressive for the last one. We can conclude that the existence of the term $\int_{\Gamma_{part}} |\mathbf{y} - \mathbf{y}_d|^2$ is crucial for a good velocity and WSS approximations. Also that is better to have the term $\int_{\Gamma_{wall}} |w - w_d|^2$ in the cost function when comparing with its absence.

Let is now consider the so called regularization term $\int_{\Gamma_{in}} |\nabla \mathbf{u}|^2$. It is clear, by observing table 3, that the cost function value is highly affected by this term, as we can see when we change the value of w_3 maintaining w_1 and w_2. Also we can observe that if $w_3 = 0$ we have good approximations for velocity and WSS, once the minimization only concerns the remaining terms. However, the absence of a regularization term may possible induce a spurious minimum (see for instance [14]). This is the case here as we can confirm in figure 5, with the picture on the right. The optimal control for $w_3 = 0$ is highly irregular and far from the parabolic profile. Thus although it corresponds to a minimum for the discrete control problem, it does not represent an admissible control function for our DA problem.

Looking at the three tables we can conclude that, within the tests we have considered (less than 400 SNOPT total iterations), the set of parameters corresponding to better approximations is $(1e^7, 1e^7, 1e^{-3})$. However we need 381 iterations to find the optimal solution, which corresponds to a large computation time. To set a reasonable balance between accuracy and computational effort, and since the weights

$$(w_1, w_2, w_3) = (1e^6, 1e^6, 1e^{-3}) \tag{17}$$

also perform very well, while taking only 281 iterations to minimize, we set this as our reference choice for the DA problem. Therefore, during the remainder, we will focus in showing how the set (17) can perform better then the limit cases, when one the weights is null.

This is the purpose, of figures 4 and 5 where we represent the optimal controls versus the inlet profile used to generate $\mathbf{y}_d$.

To compare the effect of the different choices of parameter, not only in the minimization of each term, but in the quality of the velocity approximation, we also report in table 4 both relative and absolute errors given by

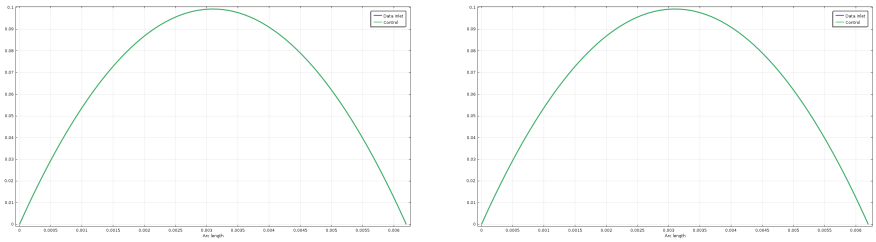

Figure 4: Left: control for $(1e^6, 1e^6, 1e^{-3})$; right: control for $(1e^6, 0, 1e^{-3})$.

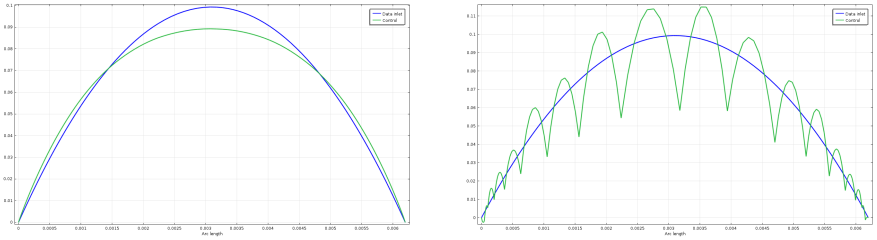

Figure 5: Left: control for $(0, 1e^6, 1e^{-3})$; right: control for $(1e^6, 1e^6, 0)$.

$$R_e = \frac{\|\mathbf{y} - \mathbf{y}_d\|_2}{\|\mathbf{y}_d\|_2} \quad \text{and} \quad A_e = \|\mathbf{y} - \mathbf{y}_d\|_2,$$

where $\|\cdot\|_2$ is the $\mathbf{L}^2$ norm.

Table 4: Relative and absolute errors for different parameters computed in Γ_{part}.

Derived Values	$(0, 1e^6, 1e^{-3})$	$(1e^6, 1e^6, 1e^{-3})$	$(1e^6, 0, 1e^{-3})$	$(1e^6, 1e^6, 0)$
R_e	0.037254	$2.709809e^{-5}$	$2.729791e^{-5}$	$1.419653e^{-5}$
A_e	$6.443602e^{-4}$	$4.687041e^{-7}$	$4.721603e^{-7}$	$2.455514e^{-7}$

We can easily confirm that the worst cost function is the one for which the velocity term is missing, and that it is better to have the WSS term than not to having it.

We have concluded that solving the control problem with (17) is our best option, within certain computational effort limit. For illustration, we represent in figures

6 - 10 the velocity, pressure, and WSS magnitude corresponding to the optimal solution. We compare this with the solution from which we took the observations y_d and w_d.

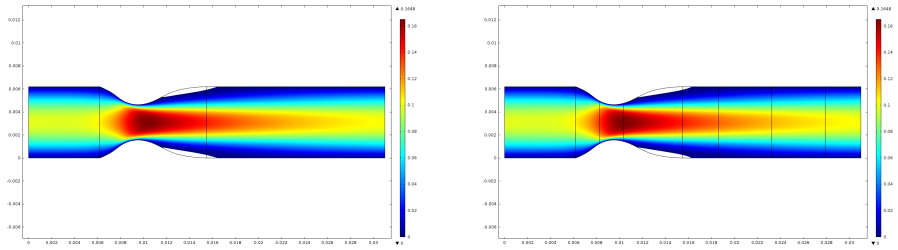

Figure 6: leff: Data velocity highlighting the recirculation region. right: controlled velocity highlighting the recirculation region

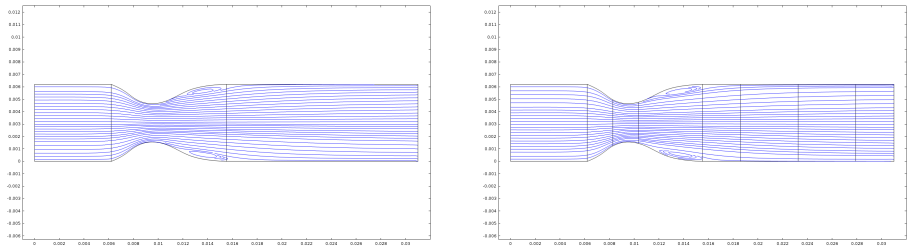

Figure 7: leff: Data velocity streamlines. right: controlled velocity streamlines

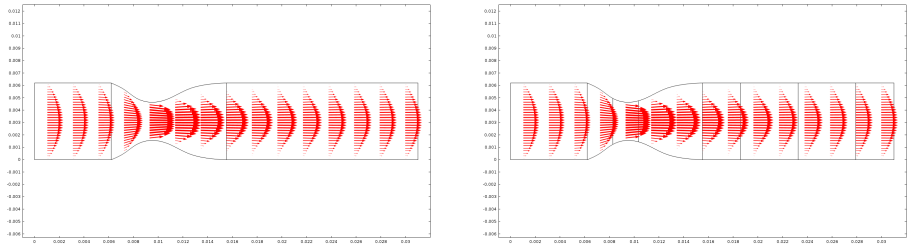

Figure 8: leff: Data velocity profile. right: controlled velocity profile

We can see that, graphically, the original solution was perfectly reconstructed from the observations.

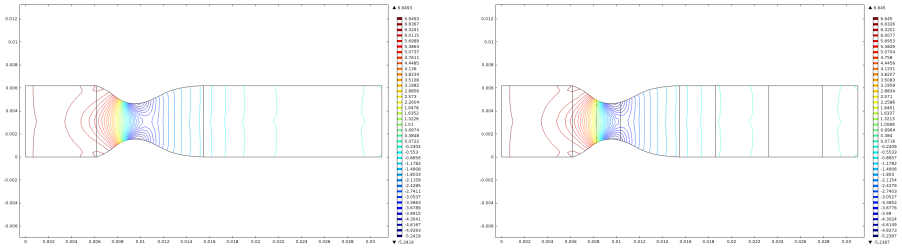

Figure 9: leff: Data pressure contour. right: controlled pressure contour

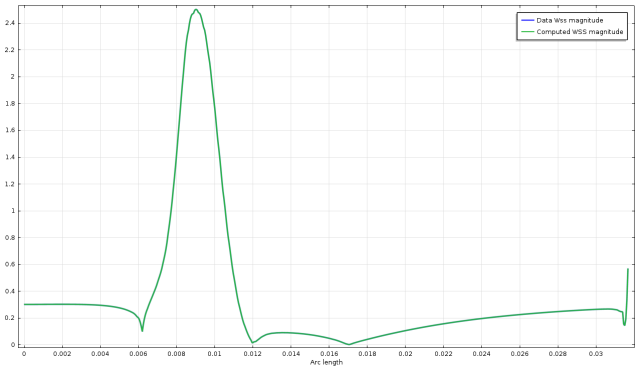

Figure 10: Controlled WSS magnitude

5.2 Robusteness of the parameters

5.2.1 Robustness to data inlet profile

To attest the robustness of the DA method, with the set of weights (17), with respect to different velocity profiles, we test different data using a power law inlet profile (see [21]) given by

$$\frac{\xi+2}{\xi}U_0\left(1-\left(\frac{y-R}{R}\right)^{\xi}\right). \tag{18}$$

Note that, for $\xi = 2$, expression (18) becames the particular case of Poiseuille flow. For our simulations we considered $\xi = 4$ and $\xi = 9$ whose profiles are represented in figure 11. U_0 was chosen such that the Reynolds number is kept equal to 180, as above. We tested $\xi = 9$ once it is commonly considered for simulating blood flow in arteries [21], and $\xi = 4$ once it is a intermediate value between 2 and 9.

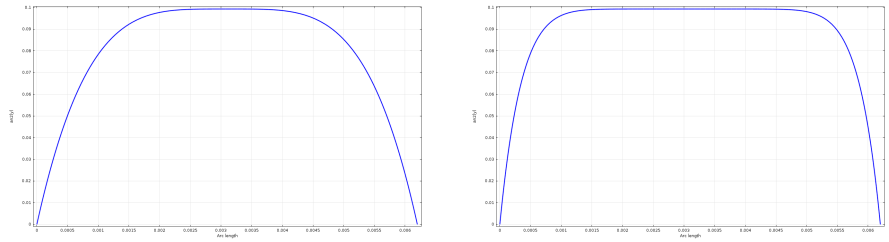

Figure 11: left: Power law with $\xi = 4$; right: Power law with $\xi = 9$.

Like in the previous section we compare the set of parameters (17) with the limit cases. The quantitative results are those in the tables 5 and 6. Similar conclusions can be inferred for both profiles. The importance of the WSS term in the cost function is more expressive when compared with the parabolic profile. To confirm these conclusions see table 7 and 8 where relative and absolute errors are compared.

Table 5: Power-Law profile, $\xi = 4$.

$\xi = 4$	$\int_{\Gamma_{part}} \lvert Y\rvert^2$	$\int_{\Gamma_{wall}} \lvert W\rvert^2$	$\int\limits_{\Gamma_{in}} \lvert\nabla \mathbf{u}\rvert^2$	CF
$(0, 1e^6, 1e^{-3})$	$1.017793e^{-6}$	$2.595413e^{-13}$	13.747798	0.0137480578
$(1e^6, 1e^6, 1e^{-3})$	$2.083886e^{-12}$	$1.033918e^{-12}$	14.513515	0.0145166331
$(1e^6, 0, 1e^{-3})$	$7.946703e^{-11}$	$7.098585e^{-8}$	14.168067	0.0142475338
$(1e^6, 1e^6, 0)$	$6.535708e^{-12}$	$1.204306e^{-11}$	392.3837	$1.8578771535e^{-5}$

Table 6: Power-Law profile, $\xi = 9$.

$\xi = 9$	$\int_{\Gamma_{part}} \lvert Y\rvert^2$	$\int_{\Gamma_{wall}} \lvert W\rvert^2$	$\int_{\Gamma_{in}} \lvert\nabla \mathbf{u}\rvert^2$	CF
$(0, 1e^6, 1e^{-3})$	$1.001349e^{-5}$	$3.259272e^{-13}$	20.106642	0.020106968
$(1e^6, 1e^6, 1e^{-3})$	$7.801032e^{-11}$	$2.094571e^{-11}$	29.855718	0.0299546736
$(1e^6, 0, 1e^{-3})$	$7.960777e^{-10}$	$1.294974e^{-6}$	24.151194	0.0249472714
$(1e^6, 1e^6, 0)$	$1.582331e^{-15}$	$7.475844e^{-22}$	565.871393	$1.582331e^{-9}$

Table 7: Relative and absolute errors for $\xi = 4$ computed in Γ_{part}.

$\xi = 4$	$(0, 1e^6, 1e^{-3})$	$(1e^6, 1e^6, 1e^{-3})$	$(1e^6, 0, 1e^{-3})$	$(1e^6, 1e^6, 0)$
R_e	0.048416	$6.927796e^{-5}$	$4.278107e^{-4}$	$1.226887e^{-4}$
A_e	0.001009	$1.443567e^{-6}$	$8.914428e^{-6}$	$2.556503e^{-6}$

Table 8: Relative and absolute errors for $\xi = 9$ computed in Γ_{part}.

$\xi = 9$	$(0, 1e^6, 1e^{-3})$	$(1e^6, 1e^6, 1e^{-3})$	$(1e^6, 0, 1e^{-3})$	$(1e^6, 1e^6, 0)$
R_e	0.134635	$3.757856e^{-4}$	0.0012	$1.692438e^{-6}$
A_e	0.003164	$8.832345e^{-6}$	$2.821485e^{-5}$	$3.977852e^{-8}$

Furthermore, the only cost function, that provides an adjustment of the control function with the original inlet profile, is precisely the one defined by (17). We can also see that such adjustment is less precise for $\xi = 9$. Figures 12 and 13 illustrate these conclusions.

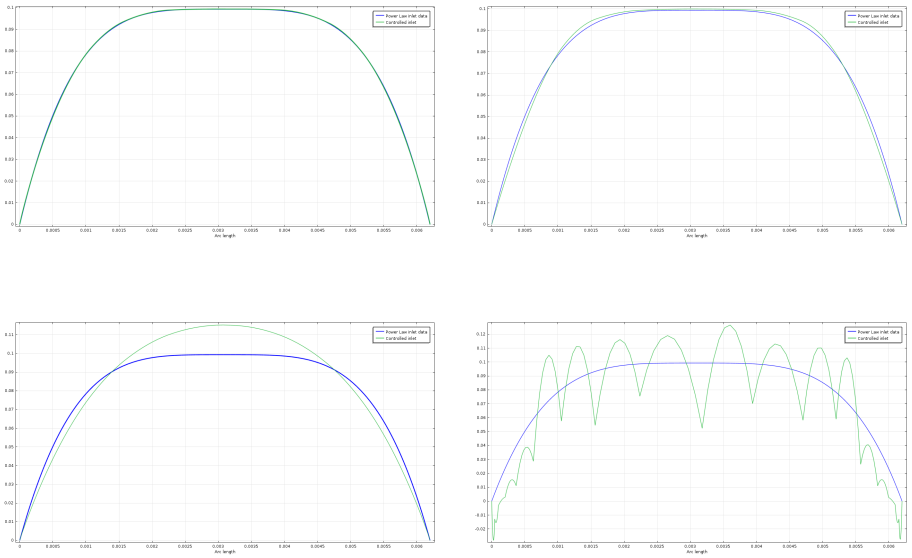

Figure 12: Power law with $\xi = 4$; upper left corner: $(1e^6, 1e^6, 1e^{-3})$, upper right corner: $(1e^6, 0, 1e^{-3})$, bottom left corner: $(0, 1e^6, 1e^{-3})$, bottom right corner $(1e^6, 1e^6, 0)$.

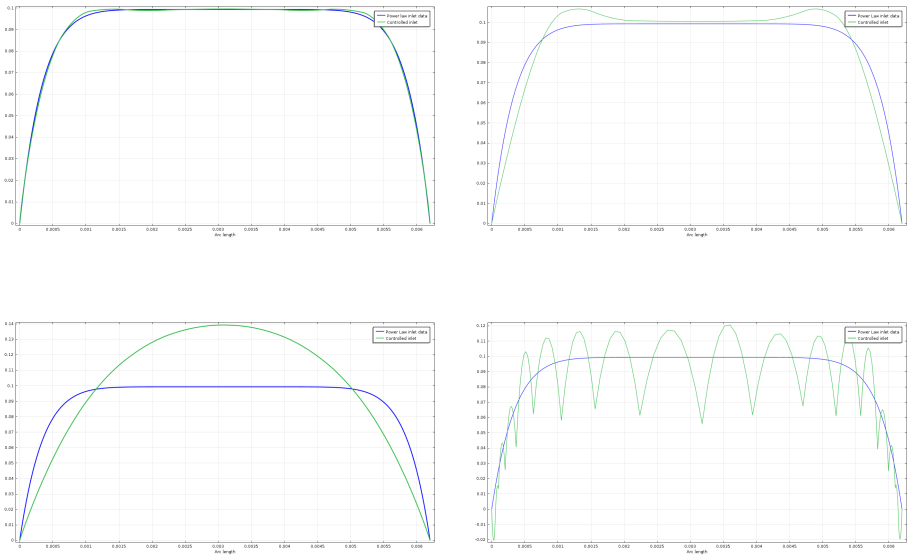

Figure 13: Power law with $\xi = 9$; upper left corner: $(1e^6, 1e^6, 1e^{-3})$, upper right corner: $(1e^6, 0, 1e^{-3})$, bottom left corner: $(0, 1e^6, 1e^{-3})$, bottom right corner $(1e^6, 1e^6, 0)$.

Finally, in table 9 we compare the errors for the different velocity profiles, obtained with our choice of parameters 17. We can see that the DA problem solved with any one of the three inlet conditions give us good approximations for the velocity field.

Table 9: Relative and absolute errors for different inlet profiles, computed in Γ_{part} for (17).

Derived Values	Poiseuille	Power-Law $\xi = 4$	Power-Law $\xi = 9$
R_e	$2.709809e^{-5}$	$6.927796e^{-5}$	$3.757856e^{-4}$
A_e	$4.687041e^{-7}$	$1.443567e^{-6}$	$8.832345e^{-6}$

Nevertheless, the closer we are to Poiseuille inlet profile, the better relative and absolute errors become.

5.2.2 Robustness to stenosis degree

In this section we compare the control problem solutions obtained for the cost function with (17) in four geometries, three different stenosis degree and no stenosis (channel). The four geometries are represented in figure 14.

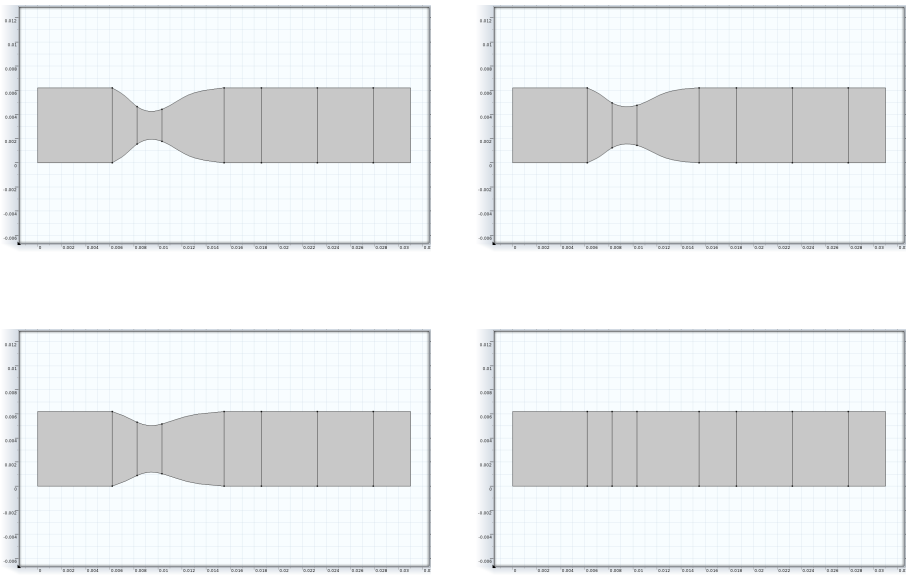

Figure 14: Upper leff corner: stenosis with $d = 3R/4$, upper right corner: stenosis with $d = R$, bottom left corner: stenosis with $d = 5R/4$, bottom right corner: channel. For all $L = 10R$ and $D = 2R$. Dofs: 96154.

We intend to show that our choice for parameters given by (17) obtained in

the section 5.1 is robust with respect to the geometries changes. In fact, even changing the geometry, we can see that a numerical solution for optimal control problem can be found, and that the original velocity is pretty well approximated, as shown by the relatives and absolute errors in table 10.

Table 10: Comparison between the three different stenosis and channel regarding the cost function value, relative and absolute errors computed in Γ_{part}.

Derived values	$3R/4$	R	$5R/4$	**channel**
CF	0.0084819835	0.0084819208	0.0084818721	0.0084818125
R_e	$2.068563e^{-5}$	$2.709878e^{-5}$	$3.19736e^{-5}$	$3.803092e^{-5}$
A_e	$3.960592e^{-7}$	$4.687051e^{-7}$	$5.176455e^{-7}$	$5.703546e^{-7}$

5.3 Effect of noise filtering

In this section we study the effect of our DA method in filtering the noise that can be added to the observed data y_d. In real applications this can be due to many different reasons, such as lack of accuracy of the observation devices or intrinsic errors of the model. Here noise samples were generated in a random way, normally distributed, with zero mean and standard deviation equal to $\bar{\sigma}_1 = 0.05\frac{U_0}{3}$, $\bar{\sigma}_2 = 0.1\frac{U_0}{3}$ and $\bar{\sigma}_3 = 0.2\frac{U_0}{3}$, respectively. For the data we use the reference stenosis geometry with radius and the velocity profile as described in the left picture of figure 2. However we include also in Γ_{part} the inlet boundary. To understand the filtering effect of the formulation (15 - 16) we compare the solution obtained with our reference set of parameters (17) with a direct approach. This approach consists in obtaining the numerical solution for the non-Newtonian model (1), by using a noisy parabolic profile, as inlet boundary condition. Such technique can be seen as the computational least expensive filtering technique when we wish to recover the solution downstream the observations. We remark, however, that it could not be used if we pretended to reconstruct the solution upstream the observed data. A similar comparison was done in [8] for Navier-Stokes equations.

The differences of the solutions obtained by filtering noise using both methods is presented in the table 11. As an index of precision, we computed a posterior, the relative error R_e and the absolute error A_e in the entire domain.
The conclusions we have for non-Newtonian problems are similar to conclusions obtained in [8] for the Newtonian problem. We can observe, as we expected, that higher values for noisy correspond to worst values for R_e and A_e.

Table 11: Comparison between controlled problem (CP) and direct problem (DP) with different noise.

Noise	Problem type	R_e (All)	A_e (All)
$\bar{\sigma} = 0.05\frac{U_0}{3}$	CP	0.001968	$2.193509e^{-6}$
	DP	0.004606	$5.134504e^{-6}$
$\bar{\sigma} = 0.1\frac{U_0}{3}$	CP	0.004974	$5.545074e^{-6}$
	DP	0.009214	$1.027040e^{-5}$
$\bar{\sigma} = 0.2\frac{U_0}{3}$	CP	0.009164	$1.021493e^{-5}$
	DP	0.018324	$2.049306e^{-5}$

6 Conclusion

In this work we proposed a DA method based on a variational approach to numerically reconstruct non-Newtonian blood flow behavior over bi-dimensional geometries.
We introduce a new cost function which takes into account the role of the WSS in the optimization process and we conclude, by testing the parameters w_1, w_2 and w_3, that this modification provides better results for velocity and WSS itself. The importance of the presence of a regularization term in the cost function was also tested. We observed that the absence of this term gives us a completely irregular control corresponding to a spurious minimum. We also proposed a set of parameters as a reasonable choice when balancing the approximation accuracy and the computational effort.

We validated the method by testing the robustness with respect to geometries change as well as new inlet profiles. In each of the cases the cost function was minimized and velocity and WSS were approximated with very small errors. Finally we tested our method as a noise filter adding three different amount of noise to the data observed solution, including inlet boundary and we compared with the Direct filtering method where the noise is added to the inlet boundary condition. The conclusions are consistent with the results obtained in [8] for Newtonian problem. A DA approach is better in correcting the noisy measurements than a Direct approach.

Acknowledgment. This work was partially supported by CMA/FCT/UNL, under the project PEst-OE/MAT/UI0297/2011, and by PTDC/MAT109973/2009.

References

[1] N. Arada *Optimal control of shear-thinning fluids*, SIAM Journal on Control and Optimization. 50, pp. 2515-2542, 2012;

[2] T. Bodnar, A. Sequeira and M. Prosi. *On the shear-thinning effects of blood flow under various flow rates*, Applied Mathematics and Computation, Elsevier, vol. 217, pp. 5055-5067, 2011.

[3] V. Calvez, J. G. Houot, N. Meunier, A. Raoult and G. Rusnakova. *Mathematical and Numerical Modeling or early atherosclerotic lesions*, ESAIM: PROCEEDINGS, Vol. 30, pp. 1-14, 2010;

[4] E. Casas, L.A. Fernandez, *Boundary control of quasilinear elliptic equations*, Rapport de Recherche 782, INRIA, 1988.

[5] E. Casas, L.A. Fernandez, *Distributed control of systems governed by a general class of quasilinear elliptic equations*, J. Differential Equations 35 (1033), pp. 20–47.

[6] J. R. Cebral, M. A. Castro, J. E. Burgess, R. S. Pergolizzi, M. J. Sheridan and C. M. Putman, Characterization of cerebral aneurysms for assessing risk of rupture by using patient-specific computational hemodynamics models, Am. J. Neuroradiol., 26 (2005), 2550-2559.

[7] M. D' Elia, M. Perego, A. Veneziani. *A Variational Data Assimilation Procedure for the Incompressible Navier-Stokes Equations in Hemodynam* ics. Journal of Scientific Computing, 2011;

[8] M. D' Elia, A. Veneziani. *A Data Assimilation technique for including noisy measurements of the velocity field into Navier-Stokes simulations.* Proceedings of V European Conference on Computational Fluid Dynamics, ECCOMAS, June 2010;

[9] M. D'Elia, A., Veneziani, A.: Methods for assimilating blood velocity measures in hemodynamics simulations: preliminary results. Proc. Comput. Sci. 1(1), 1225-1233 (2010).

[10] A. Garambuto, J. Janela, A. Moura and A. Sequeira. *Sensitivity of hemodynamics in a patient specific cerebral aneurysm to vascular geometry and blood rheology*, Mathematical Biosciences and Engineering, Volume 8, Number 2, April 2011;

[11] T. Guerra, *Distributed control for shear-thinning non-Newtonian fluids, Journal of Mathematical Fluid Mechanics*, Volume 14, 771-789, issue 4 (2012).

[12] M. Gunzburger, *Adjoint Equation-Based Methods for Control Problems in Incompressible, Viscous Flows*, Flow, Turbulence and Combustion, Vol. 65, No. 3. (1 December 2000), pp. 249-272.

[13] M. Gunzburger, C. Trenchea, *Analysis of an optimal control problem for the three-dimensional coupled modified Navier-Stokes and Maxwell equations*, J. Math. Anal. Appl. 333, pp. 295–310, 2007.

[14] J. Burkardt, M. Gunzburger, J. Peterson, *Insensitivite Functionals, Inconsistent Gradients, Spurious Minima and Regularized Funcionals in Flow*

Optimization Problems, International Journal of Computational Fluid Dynamics, 16:3, 171-185, 2002.

[15] P. Gill, W. Murray, M.A. Saunders. *SNOPT: An SQP Algoritm for Large-Scale Constrained Optimization*, Society for Industrial and Applied Mathematics, SIAM REVIEW, Vol. 47, N. I, pp 99-131, 2005;

[16] P. Gill, W. Murray, M.A. Saunders. *User's guide for SNOPT Version 7: Software for Large-Scale Nonlinear Programming*, 2008;

[17] P. Gill, W. Murray, M.A. Saunders. *User's guide for SQOPT Version 7: Software for large-scale linear and quadratic programming*, Numerical Analysis Report 06-1, Department of Mathematics, University of California San Diego, La Jolla, CA, 2006;

[18] H. Meng, Z. Wang, Y. Hoi, L. Gao, E. Metaxa, D. D. Swartz and J. Kolega, Complex hemodynamics at the apex of an arterial bifurcation induces vascular remodeling resembling cerebral aneurysm initiation, Stroke, 38 (2007), 1924-1931.

[19] *COMSOL Multiphysics, Users Guide*, COMSOL 4.3, 2012;

[20] *Optimization Module, Users Guide*, COMSOL 4.3, 2012;

[21] A. Quarteroni, L. Formaggia, Mathematical Modelling and Numerical Simulation of the Cardiovascular System, Modelling of living Systems, Handbook of Numerical Analysis Series, Elsevier, 2002.

[22] Robertson, Anne M., Sequeira, Adélia, Owens, Robert G. Rheological models for blood. Cardiovascular mathematics, 211-241, MSA. *Model. Simul. Appl.*, 1, Springer Italia, Milan, 2009.

[23] Robertson, Anne M., Sequeira, Adélia, Kameneva, M.V., Hemorheology. Hemodynamical Flows. Modeling, Analysis and Simulation, Oberwolfach Seminars, Vol. 37, 63-120, Birkhauser Verlag Basel/Switzerland, 2008.

[24] T. Slawig, *Distributed control for a class of non-Newtonian fluids*, J. Differential Equations, 219, pp. 116–143, 2005.

[25] K. Yeleswarapu, M. Kamaneva K.R. Rajagopal and J.F. Antaki, The flow of blood in tubes-theory and experiment, Mechanics Research Communication,25, 257- 262 1998.

[26] D. Wachsmuth, T. Roubíček, *Optimal control of incompressible non-Newtonian fluids*, Z. Anal. Anwend 29, pp. 351–376, 2010.